Kalman filtering technique for attitude estimation on SO(3) using single inertial vector observations

Joel Reis, Pedro Batista, *Senior Member, IEEE*,
Paulo Oliveira, *Senior Member, IEEE, Carlos Silvestre, Senior Member, IEEE*

***Abstract*— This paper presents an attitude estimation methodology for robotic platforms equipped with a set of rate gyros that can implicitly measure the Earth's rotation rate. As is well known, standard strategies for attitude determination rely on explicit body-fixed measurements of at least two inertial reference vectors. In this work, the Earth's spin is regarded as one of two constant inertial reference vectors. However, because that spin is only implicitly measured, we first implement a Kalman filter to obtain an estimate of it. This filter also yields: unbiased estimates of the second inertial reference vector, which is explicitly measured in the body-fixed frame; and estimates of two biases related to the sensor measurements. The platform's rotation matrix is then computed using a Kalman-based observer evolving on the manifold $SO(3)$ that is driven by the output of the first filter. Realistic simulation results are presented to showcase the performance of the proposed technique in two different scenarios.**

I. Introduction

In underwater environments, information is scarce and difficult to obtain/measure adequately. Not only are electromagnetic waves strongly attenuated due to water's permittivity, but also visual cues and acoustic signatures call for an unobstructed view of the water channel in order to be deemed reliable. As result, pose determination of an underwater robotic platform is a rather complex task.

The strategies found in the literature to tackle this problem are quite diverse and resort to a myriad of different sensors. But, understandably, because much work has been done around underwater acoustic technology, and on account of versatility, acoustic measurements are often a preferred source of data to help determining the orientation of an autonomous underwater vehicle (AUV).

This work was partly funded by the Macau Science and Technology Development Fund under Grant FDCT/0146/2019/A3, by the project MYRG2018-00198-FST of the University of Macau, by the Fundação para a Ciência e a Tecnologia (FCT) through LARSyS - FCT Plurianual funding 2020-2023 and through the FCT project DECENTER [LISBOA-01-0145-FEDER-029605], funded by the Programa Operacional Regional de Lisboa 2020 and PIDDAC programs.

Joel Reis and Carlos Silvestre are with the Faculty of Science and Technology, University of Macau, Taipa, Macao, China, (e-mail: {joelreis, csilvestre}@um.edu.mo).

Pedro Batista and Paulo Oliveira are with the Institute for Systems and Robotics, LARSyS, Instituto Superior Técnico, Universidade de Lisboa, 1049-001 Lisboa, Portugal, (e-mail: pbatista@isr.tecnico.ulisboa.pt, paulo.j.oliveira@tecnico.ulisboa.pt).

Paulo Oliveira is also with LAETA — Associated Laboratory for Energy, Transports and Aeronautics, IDMEC — Institute of Mechanical Engineering, Instituto Superior Técnico, Universidade de Lisboa, Lisboa 1049-001, Portugal.

Carlos Silvestre is on leave from the Instituto Superior Técnico, Universidade de Lisboa, Portugal.

For instance, the work in [5] employs a sonar to measure the locations of the underwater vehicle relative to multiple transponders; then the attitude is solved with respect to a docking platform. The authors in [10] presented an attitude filter for an Intervention-AUV working in tandem with an autonomous surface craft using measurements in body-fixed coordinates collected from an an ultra-short baseline device. More recently, [7] proposed the processing of acoustic data from a multibeam forward-looking sonar on a moving underwater platform to estimate the platform's attitude.

In [3] the authors employ velocity measurements from a Doppler velocity log to estimate acceleration to provide corrections to the accelerometer signals that improve the dynamic estimates of vehicle roll and pitch. An alternative method of estimating pitch and roll is proposed in [2], where a network of pressure sensors is used.

The work in [6] proposes using only acoustic and biased rate sensor measurements to estimate attitude according, based on the eXogenous Kalman Filter principle. Sensor bias is also taken into account in [8], where the proposed estimator is based on measuring difference in range from three or more known, fixed positions to two or more points on the AUV. Similarly, the work in [11] resorts to depth measurements to design an observer for determining a rough bias estimate. An algorithm that also makes use of depth measurements is developed in [4] to provide levels of accuracy and robustness superior to the measurements collected from an inertial measurement unit (IMU).

Within the scope of subsea scenarios, the problem with IMUs is inherent to their internal operation, which typically combines data from accelerometers, magnetometers and rate gyros. Unfortunately, when the AUV is close to large man-made metallic structures, e.g., subsea oil and gas facilities, strong magnetic signatures are likely to render the magnetometer measurements useless [9]. On the other hand, if the AUV performs a maneuver characterized by large accelerations, the accelerometer measurements also become compromised because the vehicle's acceleration is no longer known in two different references.

While in [1] a solution to overcome issues due to magnetic disturbances is proposed, in this article we develop a method that, in addition to using rate gyros that measure implicitly the planet's rotation rate, requires measurements of only one inertial reference vector. This means that our technique is extremely useful in applications where, for example, only the magnetometers or only the accelerometers can be used. In mathematical terms, we build a linear time-varying (LTV)

system and a linear time-invariant (LTI) system. The Kalman filters applied to both these linear systems form the backbone of our attitude estimator, which is then extensively validated in a realistic simulation environment.

A. Notation

Throughout this paper, a bold symbol stands for a multi-dimensional variable. Accordingly, the symbol $\mathbf{0}$ denotes a matrix of zeros and $\mathbf{I}$ an identity, both of appropriate dimensions. A block diagonal matrix is represented as $\mathrm{diag}(\mathbf{A}_1, \ldots, \mathbf{A}_n)$. In $\mathbb{R}^3$, the skew-symmetric matrix of a vector $\mathbf{a} \in \mathbb{R}^3$ is defined as $\mathbf{S}(\mathbf{a})$, such that for another vector $\mathbf{b} \in \mathbb{R}^3$ one has $\mathbf{a} \times \mathbf{b} = \mathbf{S}(\mathbf{a})\,\mathbf{b}$. The 3D rotation group is denoted by $SO(3) := \{\mathbf{X} \in \mathbb{R}^{3\times 3} : \mathbf{X}\mathbf{X}^\mathsf{T} = \mathbf{X}^\mathsf{T}\mathbf{X} = \mathbf{I} \wedge \det(\mathbf{X}) = 1\}$. $\boldsymbol{\mathcal{N}}(\boldsymbol{\mu}, \boldsymbol{\sigma})$ stands for a multivariate normal distribution with mean $\boldsymbol{\mu}$ and standard deviation $\boldsymbol{\sigma}$. For convenience, the transpose operator is denoted by the superscript $(\cdot)^\mathsf{T}$. The vector inner product is represented by $\langle \cdot, \cdot \rangle$. Variables with subscript $(\cdot)_m$ represent a measurement.

II. Theoretical Framework

To compute a rotation matrix we need information about at least two reference vectors expressed in two coordinates frames.

In this work, one frame, denoted by $\{I\}$, is assumed inertial[1], and a second frame, denoted by $\{B\}$, is one that rotates with the robotic platform. These two frames are related through a rotation matrix that transforms vectors expressed in one frame into vectors expressed in the other.

More specifically, let us denote the rotation matrix from body-fixed frame $\{B\}$ to inertial frame $\{I\}$ by $\mathbf{R}(t) \in SO(3)$. Given an initial condition $\mathbf{R}(t_0) \in SO(3)$, the evolution over time of this rotation matrix is described by

$$\dot{\mathbf{R}}(t) = \mathbf{R}(t)\mathbf{S}(\boldsymbol{\omega}(t))\,, \tag{1}$$

where $\boldsymbol{\omega}(t) \in \mathbb{R}^3$ is the angular velocity of the robotic platform; this velocity, which is expressed in $\{B\}$, describes the rotational motion of frame $\{B\}$ with respect to $\{I\}$.

The angular velocity of the robotic platform is measured by a set of rate gyros whose readings can be expressed as

$$\boldsymbol{\omega}_m(t) := \boldsymbol{\omega}(t) + \boldsymbol{\omega}_E(t) + \mathbf{b}_{\boldsymbol{\omega}} + \mathbf{n}_{\boldsymbol{\omega}}(t) \in \mathbb{R}^3, \tag{2}$$

where $\boldsymbol{\omega}_E(t) \in \mathbb{R}^3$ represents the Earth's angular velocity, $\mathbf{b}_{\boldsymbol{\omega}} \in \mathbb{R}^3$ denotes the constant rate gyro bias, and $\mathbf{n}_{\boldsymbol{\omega}}(t) \in \mathbb{R}^3$ corresponds to a noise sequence assumed white and Gaussian. All terms in (2) are expressed in frame $\{B\}$.

The implicit measurements of the Earth's spin contained in the right hand side of (2) are crucial in helping us determining the rotation matrix. Indeed, notice that

$$\boldsymbol{\omega}_E(t) = \mathbf{R}^\mathsf{T}(t)\,{}^I\boldsymbol{\omega}_E, \tag{3}$$

where ${}^I\boldsymbol{\omega}_E \in \mathbb{R}^3$ is a known reference vector representing the Earth's angular velocity expressed in inertial coordinates.

For second reference, let us consider a generic three-dimensional constant vector denoted by ${}^I\mathbf{v} \in \mathbb{R}^3$. This vector may represent, e.g., the direction of either the magnetic field or the gravitational field on the Earth's surface.

The robotic platform is thus assumed equipped with a sensor that can measure ${}^I\mathbf{v}$ in body-fixed coordinates. Let these measurements be denoted by $\mathbf{v}_m(t) \in \mathbb{R}^3$, and let the actual representation of ${}^I\mathbf{v}$ in $\{B\}$ be expressed by $\mathbf{v}(t) \in \mathbb{R}^3$. Hence, it follows that

$$\mathbf{v}_m(t) := \mathbf{v}(t) + \mathbf{b}_{\mathbf{v}} + \mathbf{n}_{\mathbf{v}}(t) \in \mathbb{R}^3, \tag{4}$$

where $\mathbf{b}_{\mathbf{v}} \in \mathbb{R}^3$ is a constant sensor bias, and $\mathbf{n}_{\mathbf{v}}(t) \in \mathbb{R}^3$ represents a sequence of noise also assumed white and Gaussian in nature.

Similar to (3), it is possible to write

$$\mathbf{v}(t) = \mathbf{R}^\mathsf{T}(t)\,{}^I\mathbf{v}. \tag{5}$$

Owing to the properties of the manifold $SO(3)$, the norm of the two reference vectors, ${}^I\boldsymbol{\omega}_E$ and ${}^I\mathbf{v}$, is invariant under rotation. Based on that, we define two positive auxiliary variable as follows:

$$\omega_E := \|\boldsymbol{\omega}_E(t)\| = \|{}^I\boldsymbol{\omega}_E\| > 0 \tag{6a}$$

$$v := \|\mathbf{v}(t)\| = \|{}^I\mathbf{v}\| > 0 \tag{6b}$$

Next, we shall decompose the Earth's angular rate vector, $\boldsymbol{\omega}_E(t)$, into two orthogonal components, such that one of them is aligned with the body-fixed representation of ${}^I\mathbf{v}$. Accordingly, let us consider the following decomposition:

$$\boldsymbol{\omega}_E(t) := \boldsymbol{\omega}_{E,\perp\mathbf{v}}(t) + \boldsymbol{\omega}_{E,\parallel\mathbf{v}}(t), \tag{7}$$

with

$$\boldsymbol{\omega}_{E,\perp\mathbf{v}}(t) := -\frac{1}{v^2}\mathbf{S}^2(\mathbf{v}(t))\,\boldsymbol{\omega}_E(t) \tag{8}$$

and

$$\boldsymbol{\omega}_{E,\parallel\mathbf{v}}(t) := \frac{\omega_E}{v}\cos(\theta)\mathbf{v}(t), \tag{9}$$

where $\theta \in (0, \pi)$ represents the angle between reference vectors ${}^I\boldsymbol{\omega}_E$ and ${}^I\mathbf{v}$. The (open) set of allowable values of θ is motivated by the following geometric assumption.

Assumption 1. *In order to avoid spatial ambiguity, the two reference vectors are assumed noncollinear, i.e., $\theta \neq 0$ and $\theta \neq \pi$ must always be verified.*

From (8), a useful constraint can be written as

$$\langle \boldsymbol{\omega}_{E,\perp\mathbf{v}}(t), \mathbf{v}(t) \rangle = 0. \tag{10}$$

Then, from equations (3), (7) and (10), a zero identity follows naturally, given by

$$\mathbf{R}^\mathsf{T}(t)\,{}^I\boldsymbol{\omega}_E - \boldsymbol{\omega}_{E,\perp\mathbf{v}}(t) - \gamma\mathbf{v}(t) = 0, \tag{11}$$

where, for notational convenience, we have defined

$$\gamma := \frac{\omega_E}{v}\cos(\theta). \tag{12}$$

[1] As a matter of fact, it rotates with the Earth, which means that there exist accelerations and, therefore, the frame is not technically inertial. However, the accelerations induced by the planet's rotation are negligible when compared to the orders of magnitude of the other quantities involved. Hence, $\{I\}$ can be regarded inertial without compromising feasibility.

III. Preliminary Kalman filter estimation

Our goal in this section is to design an estimator for the two sensor biases, for the Earth's angular velocity, and for the second reference vector. We will thus consider a system state vector defined as

$$\mathbf{x}(t) := \left[\mathbf{v}^{\mathsf{T}}(t), \quad \boldsymbol{\omega}_{E,\perp\mathbf{v}}^{\mathsf{T}}(t), \quad \mathbf{b}_{\mathbf{v}}^{\mathsf{T}}, \quad \mathbf{b}_{\boldsymbol{\omega}}^{\mathsf{T}}\right]^{\mathsf{T}} \in \mathbb{R}^{12}. \tag{13}$$

Concerning the evolution of $\mathbf{v}(t)$, the derivative of (5) can be computed nominally, i.e., without taking noise into account, as

$$\mathbf{0} = \dot{\mathbf{R}}(t)\left[\mathbf{v}_m(t) - \mathbf{b}_{\mathbf{v}}\right] + \mathbf{R}(t)\dot{\mathbf{v}}(t). \tag{14}$$

From the previous result, and using (1), we can therefore express the dynamics of $\mathbf{v}(t)$ as

$$\dot{\mathbf{v}}(t) = -\mathbf{S}(\boldsymbol{\omega}_m(t) - \boldsymbol{\omega}_{E,\perp\mathbf{v}}(t) - \mathbf{b}_{\boldsymbol{\omega}})\left[\mathbf{v}_m(t) - \mathbf{b}_{\mathbf{v}}\right]. \tag{15}$$

Likewise, the derivative of $\boldsymbol{\omega}_{E,\perp\mathbf{v}}(t)$ can be expressed as

$$\dot{\boldsymbol{\omega}}_{E,\perp\mathbf{v}}(t) = -\mathbf{S}\big(\boldsymbol{\omega}_m(t) - \boldsymbol{\omega}_{E,\|\mathbf{v}}(t) - \mathbf{b}_{\boldsymbol{\omega}}\big)\,\boldsymbol{\omega}_{E,\perp\mathbf{v}}(t), \tag{16}$$

which, according to (4), (9), and (12), may be rewritten, also nominally, as

$$\dot{\boldsymbol{\omega}}_{E,\perp\mathbf{v}}(t) = -\mathbf{S}(\boldsymbol{\omega}_m(t) - \gamma\left[\mathbf{v}_m(t) - \mathbf{b}_{\mathbf{v}}\right] - \mathbf{b}_{\boldsymbol{\omega}})\,\boldsymbol{\omega}_{E,\perp\mathbf{v}}(t). \tag{17}$$

Since our goal is to design a Kalman filter to obtain an estimate of $\mathbf{x}(t)$, we must carry out a few approximations in order to be able to formulate an LTV system.

We start by rewriting (15) as

$$\begin{aligned}\dot{\mathbf{v}}(t) = &-\mathbf{S}(\boldsymbol{\omega}_m(t))\left[\mathbf{v}_m(t) - \mathbf{b}_{\mathbf{v}}\right] \\ &+ \mathbf{S}(\boldsymbol{\omega}_{E,\perp\mathbf{v}}(t) + \mathbf{b}_{\boldsymbol{\omega}})\left[\mathbf{v}_m(t) - \mathbf{b}_{\mathbf{v}}\right].\end{aligned} \tag{18}$$

Some of the cross products in the previous equation are orders of magnitude smaller than the remaining quantities. Particularly, the term $\boldsymbol{\omega}_{E,\perp\mathbf{v}}(t) + \mathbf{b}_{\boldsymbol{\omega}}$ is always very small, especially when considering the specifications of the vast majority of commercially available high-grade rate gyros, which, on account of being designed for an accurate and reliable navigation performance, attain levels of bias instability below 1 degree per hour. Similarly, it's only sensible to assume that $\|\mathbf{b}_{\mathbf{v}}\| << \|\mathbf{v}_m(t)\|$, whereby we presume that $\mathbf{S}(\boldsymbol{\omega}_{E,\perp\mathbf{v}}(t) + \mathbf{b}_{\boldsymbol{\omega}})\,\mathbf{b}_{\mathbf{v}} \approx \mathbf{0}$. For the reasons argued before, we may also presume that $\mathbf{S}(\gamma\mathbf{b}_{\mathbf{v}} - \mathbf{b}_{\boldsymbol{\omega}})\,\boldsymbol{\omega}_{E,\perp\mathbf{v}}(t) \approx \mathbf{0}$.

Hence, equations (17) and (18) can be simplified as

$$\dot{\boldsymbol{\omega}}_{E,\perp\mathbf{v}}(t) \approx -\mathbf{S}(\boldsymbol{\omega}_m(t) - \gamma\mathbf{v}_m(t))\,\boldsymbol{\omega}_{E,\perp\mathbf{v}}(t) \tag{19}$$

and

$$\dot{\mathbf{v}}(t) \approx -\mathbf{S}(\boldsymbol{\omega}_m(t) - \boldsymbol{\omega}_{E,\perp\mathbf{v}}(t) - \mathbf{b}_{\boldsymbol{\omega}})\,\mathbf{v}_m(t) + \mathbf{S}(\boldsymbol{\omega}_m(t))\,\mathbf{b}_{\mathbf{v}}, \tag{20}$$

respectively. Finally, from (10), and by invoking the arguments leading to (19) and (20), it follows that

$$0 = \langle\boldsymbol{\omega}_{E,\perp\mathbf{v}}(t), \mathbf{v}_m(t) - \mathbf{b}_{\mathbf{v}}\rangle \approx \langle\boldsymbol{\omega}_{E,\perp\mathbf{v}}(t), \mathbf{v}_m(t)\rangle. \tag{21}$$

We have thus reunited the conditions to define a general LTV system which, in view of the state vector given in (13), can be written as

$$\begin{cases}\dot{\mathbf{x}}(t) = \mathbf{A}(t)\mathbf{x}(t) + \mathbf{B}(t)\mathbf{v}_m(t) + \mathbf{w}(t) \\ \mathbf{y}(t) = \mathbf{C}(t)\mathbf{x}(t) + \mathbf{n}(t)\end{cases}, \tag{22}$$

where

$$\mathbf{A}(t) = \left[\begin{array}{cc|c} \mathbf{0} & \mathbf{0} & \\ \mathbf{S}(\mathbf{v}_m(t)) & \mathbf{S}(\boldsymbol{\omega}_m(t) - \gamma\mathbf{v}_m(t)) & \mathbf{0} \\ -\mathbf{S}(\boldsymbol{\omega}_m(t)) & \mathbf{0} & \\ \mathbf{S}(\mathbf{v}_m(t)) & \mathbf{0} & \end{array}\right]^{\mathsf{T}} \in \mathbb{R}^{12\times 12}, \tag{23}$$

$$\mathbf{B}(t) = \begin{bmatrix}-\mathbf{S}(\boldsymbol{\omega}_m(t)) \\ \mathbf{0}\end{bmatrix} \in \mathbb{R}^{12\times 3}, \quad \mathbf{y}(t) = \begin{bmatrix}\mathbf{v}_m(t) \\ 0\end{bmatrix} \in \mathbb{R}^{4}, \tag{24}$$

$$\mathbf{C}(t) = \begin{bmatrix}\mathbf{I} & \mathbf{0} & \mathbf{I} & \mathbf{0} \\ \mathbf{0} & \mathbf{v}_m^{\mathsf{T}}(t) & \mathbf{0} & \mathbf{0}\end{bmatrix} \in \mathbb{R}^{4\times 12}, \tag{25}$$

and, finally, where $\mathbf{w}(t) \in \mathbb{R}^{12}$, with $\mathbf{w}(t) \sim \boldsymbol{\mathcal{N}}(\mathbf{0}, \boldsymbol{\mathcal{Q}})$, and $\mathbf{n}(t) \in \mathbb{R}^4$, with $\mathbf{n}(t) \sim \boldsymbol{\mathcal{N}}(\mathbf{0}, \boldsymbol{\mathcal{R}})$, represent the zero-mean process noise and the observations noise, respectively. In turn, the matrices $\boldsymbol{\mathcal{Q}} \in \mathbb{R}^{12\times 12}$, $\boldsymbol{\mathcal{Q}} \succ \mathbf{0}$, and $\boldsymbol{\mathcal{R}} \in \mathbb{R}^{4\times 4}$, $\boldsymbol{\mathcal{R}} \succ \mathbf{0}$, represent noise covariances associated with different white Gaussian noise distributions. These matrices can be seen as tuning knobs to adjust the estimation performance.

The zero element of $\mathbf{y}(t)$ acts as a constraint on the LTV system (22) that has positive impact on the observability.

Following the definition of the system state vector presented in (13), we let its estimate be denoted by

$$\widehat{\mathbf{x}}(t) := \left[\widehat{\mathbf{v}}^{\mathsf{T}}(t), \quad \widehat{\boldsymbol{\omega}}_{E,\perp\mathbf{v}}^{\mathsf{T}}(t), \quad \widehat{\mathbf{b}}_{\mathbf{v}}^{\mathsf{T}}(t), \quad \widehat{\mathbf{b}}_{\boldsymbol{\omega}}^{\mathsf{T}}(t)\right]^{\mathsf{T}} \in \mathbb{R}^{12}. \tag{26}$$

Therefore, a classic Kalman filter for the LTV system (22) is given by

$$\begin{cases}\dot{\widehat{\mathbf{x}}}(t) = \mathbf{A}(t)\widehat{\mathbf{x}}(t) + \mathbf{B}(t)\mathbf{v}_m(t) \\ \qquad\qquad + \boldsymbol{\mathcal{K}}(t)\left[\mathbf{y}(t) - \mathbf{C}(t)\widehat{\mathbf{x}}(t)\right], & \text{(27a)} \\ \boldsymbol{\mathcal{K}}(t) = \mathbf{P}(t)\mathbf{C}^{\mathsf{T}}(t)\boldsymbol{\mathcal{R}}^{-1}, & \text{(27b)} \\ \dot{\mathbf{P}}(t) = -\mathbf{P}(t)\mathbf{C}^{\mathsf{T}}(t)\boldsymbol{\mathcal{R}}^{-1}\mathbf{C}(t)\mathbf{P}(t) \\ \qquad\qquad + \mathbf{A}(t)\mathbf{P}(t) + \mathbf{P}(t)\mathbf{A}^{\mathsf{T}}(t) + \boldsymbol{\mathcal{Q}}. & \text{(27c)}\end{cases}$$

The initial condition of the Riccati matrix differential equation (27c), expressed by $\mathbf{P}(t_0) \succ \mathbf{0}$, plays an important role since it can be tuned to adjust the filter's performance, in particular concerning convergence speed. As argued in [12], in addition to cross-term approximations, the system matrices $\mathbf{A}(t)$, $\mathbf{B}(t)$, and $\mathbf{C}(t)$ are sources of cross-correlated sensor noise, whereby the filter may only be deemed sub-optimal.

According to (7), and by using the output of the Kalman filter (27), i.e., $\widehat{\mathbf{x}}(t)$, an estimate of the Earth's spin expressed in frame $\{B\}$ can be computed as

$$\widehat{\boldsymbol{\omega}}_E(t) = \widehat{\boldsymbol{\omega}}_{E,\perp\mathbf{v}}(t) + \gamma\widehat{\mathbf{v}}(t). \tag{28}$$

IV. Attitude Observer on $SO(3)$

Now that we have in hand two known inertial reference vectors, namely ${}^{I}\boldsymbol{\omega}_E$ and ${}^{I}\mathbf{v}$, as well as estimates of their body-fixed counterparts, we can resort to any conventional attitude observer in order to determine $\mathbf{R}(t)$. However, because most of these solutions consist in deterministic observers that rely on a fine tuning of (piecewise) constant scalar gains, herein we shall employ a slightly modified version of the observer proposed by the authors in [13], whose time-varying matrix gain stems from Kalman filtering theory.

The dynamics of the proposed observer, whose initial condition satisfies $\widehat{\mathbf{R}}(t_0) \in SO(3)$, evolves on the manifold and is given by

$$\dot{\widehat{\mathbf{R}}}(t) := \widehat{\mathbf{R}}(t)\mathbf{S}(\widehat{\boldsymbol{\omega}}(t) + \boldsymbol{\xi}(t)), \tag{29}$$

where

$$\widehat{\boldsymbol{\omega}}(t) := \boldsymbol{\omega}_m(t) - \widehat{\mathbf{R}}^{\mathsf{T}}(t)\,{}^I\boldsymbol{\omega}_E - \widehat{\mathbf{b}}_{\boldsymbol{\omega}}(t) \in \mathbb{R}^3, \tag{30}$$

and

$$\boldsymbol{\xi}(t) := \widehat{\mathbf{R}}^{\mathsf{T}}(t)\mathbf{K}(t)\widehat{\mathbf{R}}(t)\mathbf{S}(\widehat{\mathbf{v}}(t))\,\widehat{\mathbf{R}}^{\mathsf{T}}(t)\,{}^I\mathbf{v} \in \mathbb{R}^3, \tag{31}$$

with $\mathbf{K}(t) \in \mathbb{R}^{3\times 3}$ representing a matrix gain to be determined. Based on (1), the structure of (29) is quite intuitive: $\widehat{\boldsymbol{\omega}}(t)$ constitutes an estimate of the robotic platform's angular velocity while $\boldsymbol{\xi}(t)$ ultimately conveys a correction term in the form of an axis and angle of rotation.

When working on the manifold $SO(3)$, an attitude estimation error should also consist in a rotation matrix. Indeed, that error should express how much and about which direction should we rotate our estimated vectors in order to rectify their body-fixed representations. Hence, let us define

$$\widetilde{\mathbf{R}}(t) := \mathbf{R}(t)\widehat{\mathbf{R}}^{\mathsf{T}}(t) \in SO(3). \tag{32}$$

Notice that when $\widehat{\mathbf{R}}(t) \equiv \mathbf{R}(t)$, the error rotation matrix becomes the identity transformation, i.e., $\mathbf{I}$.

According to (29) and (32), the dynamics of the error rotation matrix, i.e., $\dot{\widetilde{\mathbf{R}}}(t)$, follows as (cf. [13] for detailed steps)

$$\begin{aligned}\dot{\widetilde{\mathbf{R}}}(t) = \widetilde{\mathbf{R}}(t)\mathbf{S}\Big(\Big[\mathbf{I} - \widetilde{\mathbf{R}}^{\mathsf{T}}(t)\Big]\,{}^I\boldsymbol{\omega}_E - \widehat{\mathbf{R}}(t)\widetilde{\mathbf{b}}_{\boldsymbol{\omega}}(t)\Big) \\ - \widetilde{\mathbf{R}}(t)\mathbf{S}\Big(\mathbf{K}(t)\mathbf{S}\Big(\Big[\widetilde{\mathbf{R}}^{\mathsf{T}}(t)\,{}^I\mathbf{v} + \widehat{\mathbf{R}}(t)\widetilde{\mathbf{b}}_{\mathbf{v}}(t)\Big]\Big)\,{}^I\mathbf{v}\Big).\end{aligned} \tag{33}$$

All that is left now is for us to determine $\mathbf{K}(t)$. The implicit goal is to drive $\widetilde{\mathbf{R}}(t)$ to $\mathbf{I}$, as suggested by (32).

It is also convenient, especially during an error analysis, to consider the angle-axis parameterization of $\widetilde{\mathbf{R}}(t)$, which can be written (using Rodrigues' rotation formula) as

$$\widetilde{\mathbf{R}}(t) = \mathbf{I} + \sin\Big(\widetilde{\phi}(t)\Big)\,\mathbf{S}(\widetilde{\boldsymbol{\mu}}(t)) + \Big[1 - \cos\Big(\widetilde{\phi}(t)\Big)\Big]\,\mathbf{S}^2(\widetilde{\boldsymbol{\mu}}(t)), \tag{34}$$

where $\widetilde{\phi}(t) \in [0, \pi]$ and unit vector $\widetilde{\boldsymbol{\mu}}(t)$ form an angle-axis pair. Hence, $\mathbf{K}(t)$ should be such that, according to (34), $\widetilde{\phi}(t)$ converges to zero as times goes to infinity.

Consider then the continuous-time LTI system

$$\begin{cases}\dot{\boldsymbol{x}}(t) = -\mathbf{S}\big({}^I\boldsymbol{\omega}_E\big)\,\boldsymbol{x}(t) + \boldsymbol{w}(t) \\ \boldsymbol{y}(t) = -\mathbf{S}^2\big({}^I\mathbf{v}\big)\,\boldsymbol{x}(t) + \boldsymbol{v}(t)\end{cases}, \tag{35}$$

where $\boldsymbol{x}(t) \in \mathbb{R}^3$ represents a state vector, and $\boldsymbol{y}(t) \in \mathbb{R}^3$ stands for an observations vector. Let $\boldsymbol{w}(t)$ and $\boldsymbol{v}(t)$ denote white Gaussian noise sequences, such that $\boldsymbol{w}(t) \sim \boldsymbol{\mathcal{N}}(\mathbf{0}, \boldsymbol{\mathcal{E}})$ and $\boldsymbol{v}(t) \sim \boldsymbol{\mathcal{N}}(\mathbf{0}, \boldsymbol{\mathcal{J}})$, where $\boldsymbol{\mathcal{E}},\ \boldsymbol{\mathcal{J}} \in \mathbb{R}^{3\times 3}$ are positive definite covariance matrices that can be fine-tuned.

The natural estimation solution for the previous LTI system is a Kalman filter. If we denote the filter output by $\widehat{\boldsymbol{x}}(t)$, then the dynamics of this output are governed by

$$\dot{\widehat{\boldsymbol{x}}}(t) = -\mathbf{S}\big({}^I\boldsymbol{\omega}_E\big)\,\widehat{\boldsymbol{x}}(t) + \mathbf{K}(t)\,\big[\boldsymbol{y}(t) + \mathbf{S}^2\big({}^I\mathbf{v}\big)\,\widehat{\boldsymbol{x}}(t)\big], \tag{36}$$

where we want $\mathbf{K}(t)$ to be the same as in (33).

Let the Kalman filter error be denoted by $\boldsymbol{e}(t) := \boldsymbol{x}(t) - \widehat{\boldsymbol{x}}(t)$. Then, using (35) and (36), the nominal dynamics of $\boldsymbol{e}(t)$ follows as

$$\dot{\boldsymbol{e}}(t) = -\big[\mathbf{S}\big({}^I\boldsymbol{\omega}_E\big) - \mathbf{K}(t)\mathbf{S}^2\big({}^I\mathbf{v}\big)\big]\,\boldsymbol{e}(t). \tag{37}$$

It is import to stress that, as shown in [13], because the LTI system is observable as long as **Assumption 1** holds, the solutions of (37) are exponentially stable. Then, as is well-known, the computation of $\mathbf{K}(t)$ follows directly from the solution of the Riccati matrix differential equation given by

$$\begin{aligned}\dot{\boldsymbol{\mathcal{P}}}(t) = &-\boldsymbol{\mathcal{P}}(t)\mathbf{S}^2\big({}^I\mathbf{v}\big)\,\boldsymbol{\mathcal{J}}^{-1}\mathbf{S}^2\big({}^I\mathbf{v}\big)\,\boldsymbol{\mathcal{P}}(t) \\ &- \mathbf{S}\big({}^I\boldsymbol{\omega}_E\big)\,\boldsymbol{\mathcal{P}}(t) + \boldsymbol{\mathcal{P}}(t)\mathbf{S}\big({}^I\boldsymbol{\omega}_E\big) + \boldsymbol{\mathcal{E}}.\end{aligned} \tag{38}$$

The formula to compute the gain follows as

$$\mathbf{K}(t) = -\boldsymbol{\mathcal{P}}(t)\mathbf{S}^2\big({}^I\mathbf{v}\big)\,\boldsymbol{\mathcal{J}}^{-1}. \tag{39}$$

In the same way as (27c), the initial condition of (38), expressed by $\boldsymbol{\mathcal{P}}(t_0) \succ \mathbf{0}$, also has impact on the estimation performance.

Up until now, we have developed a traditional Kalman filtering procedure for an LTI system, particularly (35), but its tie-in to error dynamics (33) is yet to be explained.

The small angle approximation can be exploited to obtain a linearised rotation matrix error that can be computed as

$$\widetilde{\mathbf{R}}(t) \approx \mathbf{I} + \mathbf{S}(\boldsymbol{\eta}(t)), \tag{40}$$

where $\boldsymbol{\eta}(t) \in \mathbb{R}^3$ is a vector encoding infinitesimal rotations about the three axes of coordinate frame $\{B\}$. Using (40), and assuming negligible bias errors, we can simplify (33) as

$$\dot{\widetilde{\mathbf{R}}}(t) \approx \mathbf{S}\big(-\big[\mathbf{S}\big({}^I\boldsymbol{\omega}_E\big) - \mathbf{K}(t)\mathbf{S}^2\big({}^I\mathbf{v}\big)\big]\,\boldsymbol{\eta}(t)\big). \tag{41}$$

Comparing (41) with (37), we conclude that, given $\mathbf{K}(t)$ computed in (39), the time-derivative of $\boldsymbol{\eta}(t)$, which follows from the derivative of (40) juxtaposed with (41), has the same dynamics as $\boldsymbol{e}(t)$. This means that $\boldsymbol{\eta}(t) = \mathbf{0}$ is an exponentially stable equilibrium point. As result, and according to (41), $\dot{\widetilde{\mathbf{R}}}(t)$ converges to zero. We can then show (cf. [13]) that $\widetilde{\mathbf{R}}(t)$ converges locally exponentially fast to $\mathbf{I}$.

V. Simulation Results

A. General Setup

Consider an AUV equipped with a high-performance IMU, e.g., the Fiber Optic Gyro IMU 1775 from KVH Industries. In addition to high-grade rate gyros that are accurate enough to perceive the rotation of the planet, this unit also encompasses a set of tri-axial accelerometers and a set of tri-axial magnetometers, all included in a compact design, weighing approximately 700 grams, that is relatively low-cost and of small dimensions.

Furthermore, suppose the AUV is performing a maneuver located around a latitude of $\varphi = 38.822614$ degrees (North) and a longitude of $\psi = 9.016309$ degrees (West).

In view of the local tangent North-East-Down (NED) plane, at sea level, and for the aforementioned geographic coordinates, the components of the inertial acceleration due

to gravity, and the components of the inertial magnetic field are given, according to the International Gravity Formula 1980, and to the 13th generation of the International Geomagnetic Reference Field model, respectively, by

$$ {}^{I}\mathbf{v} : \begin{cases} \begin{bmatrix} 0, & 0, & 9.800611 \end{bmatrix}^{\mathsf{T}} \ (\mathrm{m/s^2}) \\ \begin{bmatrix} 0.26571, & -0.00767, & 0.35045 \end{bmatrix}^{\mathsf{T}} \ (\mathrm{G}) \end{cases}. \tag{42} $$

In turn, concerning the sidereal day, the Earth's angular speed is approximately $\left\| {}^{I}\boldsymbol{\omega}_E \right\| = 7.2921159 \times 10^{-5}$ rad/s, or roughly 15 degrees per hour. Therefore, the Earth's rate vector expressed in the inertial NED coordinate frame $\{I\}$ can be written as

$$ {}^{I}\boldsymbol{\omega}_E = \left\| {}^{I}\boldsymbol{\omega}_E \right\| [\cos(\varphi),\ 0,\ \sin(\varphi)]^{\mathsf{T}}. \tag{43} $$

The maneuver described by the AUV is characterized by an angular velocity whose evolution over time obeys to

$$ \boldsymbol{\omega}(t) := \left[5\sin\left(\tfrac{\pi}{30}t\right), \quad \sin\left(\tfrac{\pi}{90}t\right), \quad -2\sin\left(\tfrac{\pi}{150}t\right) \right]^{\mathsf{T}} \ (\mathrm{deg/s}). \tag{44} $$

The initial attitude of the AUV is set as $\mathbf{R}(t_0) = \mathbf{I}$. Concerning the sensor measurements, and as suggested by equations (2) and (4), the noise sequences are selected to follow normal distributions, in particular, $\mathbf{n}_{\boldsymbol{\omega}}(t) \sim \boldsymbol{\mathcal{N}}(\mathbf{0}, \sigma_{\boldsymbol{\omega}}^2 \mathbf{I})$ and $\mathbf{n}_{\mathbf{v}}(t) \sim \boldsymbol{\mathcal{N}}(\mathbf{0}, \sigma_{\mathbf{v}}^2 \mathbf{I})$, where $\sigma_{\boldsymbol{\omega}}, \sigma_{\mathbf{v}} > 0$ are standard deviations whose values we set out in Table I along with other sensor specifications employed in the simulations.

TABLE I

NOISE AND BIAS SPECIFICATIONS OF THE SENSOR ENSEMBLE.

Variable	Sensor	Value	Units
$\sigma_{\boldsymbol{\omega}}$	rate gyro	0.000972	deg/s
$\sigma_{\mathbf{v}}$	accelerometer	0.6	mg
	magnetometer	0.1	mG
$\mathbf{b}_{\boldsymbol{\omega}}$	rate gyro	$[1, \ -1, \ -1]$	deg/h
$\mathbf{b}_{\mathbf{v}}$	accelerometer	$0.5[-1, \ 1, \ 1]^{\mathsf{T}}$	mg
	magnetometer	$0.2[-1, \ 1, \ 1]^{\mathsf{T}}$	mG

Across all tests carried out in the sequel, the initial condition of the first Kalman filter (27) was always set to

$$ \widehat{\mathbf{x}}(t_0) = \begin{bmatrix} \mathbf{v}_m^{\mathsf{T}}(t_0), & \mathbf{0}, & \mathbf{0}, & \mathbf{0} \end{bmatrix}^{\mathsf{T}}. \tag{45} $$

We performed two sets of simulations: one using the direction of gravity as reference vector, along with biased accelerometer measurements; another using the direction of the magnetic field, along with biased magnetometer measurements. For each set, our attitude estimation solution was run $N = 15$ times. Each run was initialized with starting angle error set as $\widetilde{\phi}(t_0) := 12i+1$ degrees, for $i = 0, 1, \ldots, N-1$, paired with a random rotation vector $\widetilde{\boldsymbol{\mu}}(t_0)$. Consequently, the initial guesstimate of the rotation matrix was computed based on equations (32) and (34).

These N algorithmic runs, each lasting 30 minutes, shall allow us to properly assess the performance of the overall attitude observer when confronted with various initial conditions. It is also important to stress that the generated additive white Gaussian noise sequences, $\mathbf{n}_{\boldsymbol{\omega}}(t)$ and $\mathbf{n}_{\mathbf{v}}(t)$, are quantitatively different for each run.

B. Accelerometer case

The covariance matrices of the two filters were empirically tuned for the best achievable performance. Their values are as follows:

$$ \begin{aligned} \mathbf{P}(t_0) &= \mathrm{diag}(10^{-2}\mathbf{I}, 10^{-5}\mathbf{I}, 10^{-2}\mathbf{I}, 10^{-5}\mathbf{I}), \\ \boldsymbol{\mathcal{Q}} &= \mathrm{diag}(10^{-8}\mathbf{I}, 10^{-10}\mathbf{I}, 10^{-12}\mathbf{I}, 10^{-12}\mathbf{I}), \\ \boldsymbol{\mathcal{R}} &= \mathrm{diag}(10^{-3}\mathbf{I}, 10^{-4}), \\ \boldsymbol{\mathcal{P}}(t_0) &= 10\mathbf{I}, \ \boldsymbol{\mathcal{E}} = 5 \times 10^{-12}\mathbf{I}, \ \text{and} \ \boldsymbol{\mathcal{J}} = 10^{-4}\mathbf{I}. \end{aligned} \tag{46} $$

Note that these matrices remain the same across the N simulation runs, which is rather advantageous to this type of application, as we don't have to adjust the filter in function of the problem's initial conditions.

Figure 1 displays the evolution of the angle error $\widetilde{\phi}(t)$ for all N runs. A relatively quick transient response is verified across all sequences. We can also observe that the steady-state behavior, in particular the magnitude of the error, is not directly linked to the initial angle deviation. This suggests, as expected, that the starting rotation error vector $\widetilde{\boldsymbol{\mu}}(t_0)$, as well as the output of the first Kalman filter, impact on the performance of observer (29).

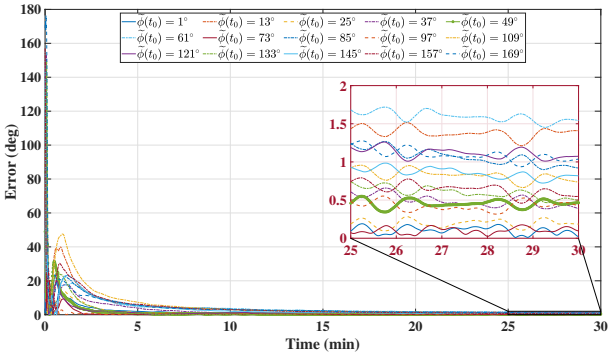

Fig. 1. Evolution of $\widetilde{\phi}(t)$ sequences (accelerometer case).

Figure 2 showcases the evolution of $\|\widetilde{\boldsymbol{\omega}}_E(t)\|$ for all N runs. The steady-state magnitude of the errors, for $t \geq 3$ min, compares well with the speed of the Earth's spin, which, we recall, is approximately 15 degrees per hour.

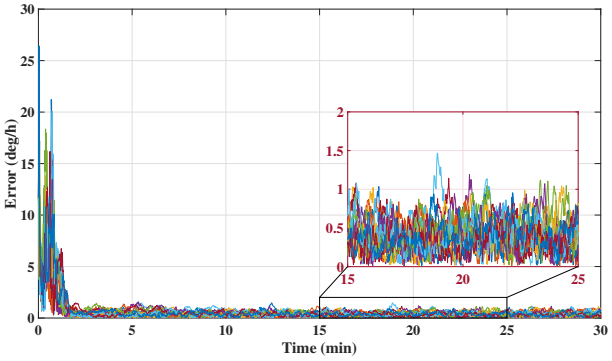

Fig. 2. Evolution of $\|\widetilde{\boldsymbol{\omega}}_E(t)\|$ sequences (accelerometer case).

Figures 3 and 4 illustrate the evolution of the norm of $\widetilde{\mathbf{b}}_{\mathbf{v}}(t)$ and $\widetilde{\mathbf{b}}_{\boldsymbol{\omega}}(t)$, respectively. The estimation of $\mathbf{b}_{\mathbf{v}}$ is notoriously more accurate than that of $\mathbf{b}_{\boldsymbol{\omega}}$. This is in line with

the structure of LTV system (22), which relates $\widehat{\mathbf{b}}_{\mathbf{v}}(t)$ with the system observations through matrix $\mathbf{C}(t)$. Furthermore, the approximations that were carried out in regard to cross-terms involving the sensor biases and the Earth's spin are ultimately a bottleneck in the system. These drawbacks will be tackled in future work.

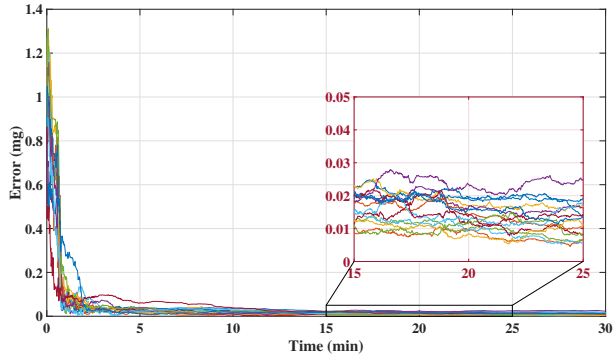

Fig. 3. Evolution of $\|\widetilde{\mathbf{b}}_{\mathbf{v}}(t)\|$ sequences (accelerometer case).

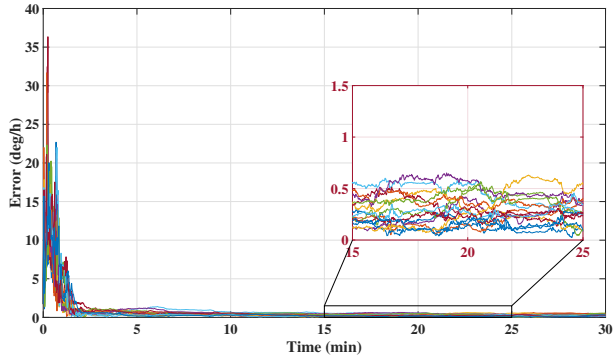

Fig. 4. Evolution of $\|\widetilde{\mathbf{b}}_{\boldsymbol{\omega}}(t)\|$ sequences (accelerometer case).

C. Magnetometer case

Due to different noise and magnitude levels involved in the magnetometer case, as seen from Table I, the covariance matrices of the two filters were adjusted as follows:

$$\begin{aligned} \mathbf{P}(t_0) &= \mathrm{diag}(10^{-4}\mathbf{I}, 10^{-7}\mathbf{I}, 10^{-5}\mathbf{I}, 10^{-6}\mathbf{I}), \\ \boldsymbol{\mathcal{Q}} &= \mathrm{diag}(10^{-8}\mathbf{I}, 10^{-14}\mathbf{I}, 10^{-12}\mathbf{I}, 10^{-16}\mathbf{I}), \\ \boldsymbol{\mathcal{R}} &= \mathrm{diag}(10^{-7}\mathbf{I}, 10^{-6}), \\ \boldsymbol{\mathcal{P}}(t_0) &= \mathbf{I},\ \boldsymbol{\mathcal{E}} = 5\times 10^{-11}\mathbf{I},\ \text{and}\ \boldsymbol{\mathcal{J}} = 10^{-6}\mathbf{I}. \end{aligned} \tag{47}$$

Overall, the qualitative and quantitative analysis reported in the previous section for the accelerometer case can be extended, in every detail, to the magnetometer case. Nevertheless, for the sake of completeness and for reference, we are presenting below an equal number of plots displaying the evolution of the same errors.

VI. Conclusions

This paper addressed the problem of attitude estimation using rate gyros that implicitly measure the Earth's spin, and using body-fixed measurements of a known constant inertial reference vector. A Kalman filter was first developed to obtain an estimate of the Earth's angular velocity expressed

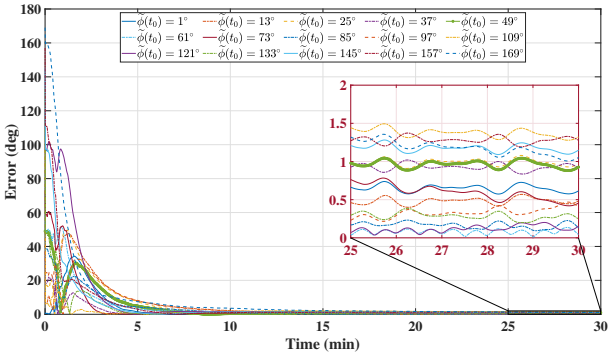

Fig. 5. Evolution of $\widetilde{\phi}(t)$ sequences (magnetometer case).

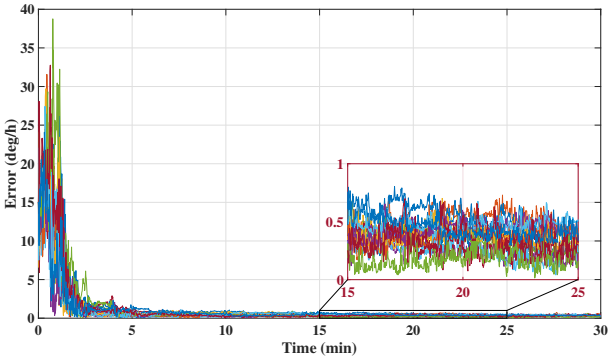

Fig. 6. Evolution of $\|\widetilde{\boldsymbol{\omega}}_E(t)\|$ sequences (magnetometer case).

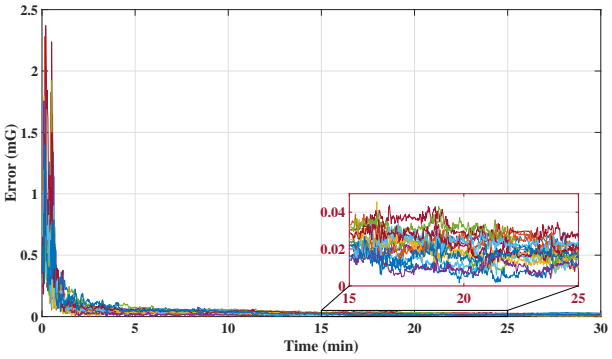

Fig. 7. Evolution of $\|\widetilde{\mathbf{b}}_{\mathbf{v}}(t)\|$ sequences (magnetometer case).

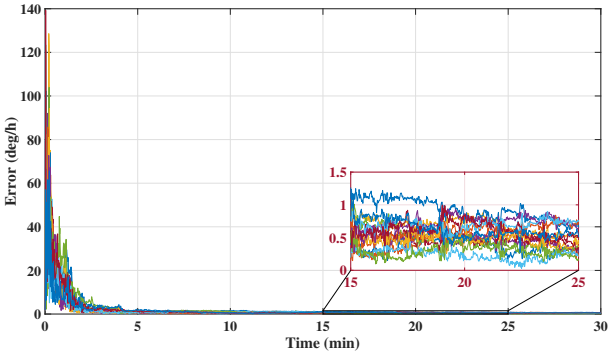

Fig. 8. Evolution of $\|\widetilde{\mathbf{b}}_{\boldsymbol{\omega}}(t)\|$ sequences (magnetometer case).

in body-fixed coordinates, as well as to obtain estimates of two sensor biases. The output of this filter was then forwarded to a rotation matrix observer built on the manifold $SO(3)$. The observer dynamics is a function of a matrix gain stemming from a Kalman filter applied to an auxiliary linear time-invariant system. At last, the proposed solution, which is simple in structure and easy to tune, was validated through two sets of realistic simulations.

REFERENCES

[1] B. Allotta, R. Costanzi, F. Fanelli, N. Monni, and A. Ridolfi. Underwater Vehicles attitude estimation in presence of magnetic disturbances. In *2016 IEEE International Conference on Robotics and Automation (ICRA)*. IEEE, May 2016.

[2] A. Baruch, Y. Mazal, B. Braginsky, and H. Guterman. Attitude Estimation of AUVs Based on a Network of Pressure Sensors. *IEEE Sensors Journal*, 20(14):7988–7996, July 2020.

[3] G. Troni and L. L. Whitcomb. Preliminary experimental evaluation of a Doppler-aided attitude estimator for improved Doppler navigation of underwater vehicles. In *2013 IEEE International Conference on Robotics and Automation*. IEEE, May 2013.

[4] N. Y. Ko, H. T. Choi, C.-M. Lee, and Y. S. Moon. Attitude estimation using depth measurement and AHRS data for underwater vehicle navigation. In *OCEANS 2016 - Shanghai*, pages 1–4, 2016.

[5] D. Sun, C. Zheng, D. Zhang, and J. Zhang. A high accuracy position and attitude measure sonar for submarine docking. In *2013 OCEANS - San Diego*, pages 1–6, 2013.

[6] E. K. Jørgensen and I. Schjølberg. Attitude and Rate Sensor Bias Estimation for Underwater Vehicles. In *2018 26th Mediterranean Conference on Control and Automation (MED)*, pages 1–7, 2018.

[7] B. T. Henson and Y. V. Zakharov. Attitude-Trajectory Estimation for Forward-Looking Multibeam Sonar Based on Acoustic Image Registration. *IEEE Journal of Oceanic Engineering*, 44(3):753–766, July 2019.

[8] E. K. Jørgensen and I. Schjølberg. Attitude and Gyro bias estimation using range-difference and IMU measurements. In *2016 IEEE/OES Autonomous Underwater Vehicles (AUV)*, pages 124–130, 2016.

[9] B. B. Stovner and T. A. Johansen. Hydroacoustically aided inertial navigation for joint position and attitude estimation in absence of magnetic field measurements. In *2017 American Control Conference (ACC)*, pages 1211–1218, 2017.

[10] M. Morgado, P. Batista, P. Oliveira, and C. Silvestre. Attitude Estimation for Intervention-AUVs Working in Tandem with Autonomous Surface Craft. *European Journal of Control*, 18(5):485–495, January 2012.

[11] E. K. Jørgensen, T. I. Fossen, T. H. Bryne, and I. Schjølberg. Underwater Position and Attitude Estimation Using Acoustic, Inertial, and Depth Measurements. *IEEE Journal of Oceanic Engineering*, 45(4):1450–1465, October 2020.

[12] J. Reis, P. Batista, P. Oliveira, and C. Silvestre. Attitude, body-fixed Earth rotation rate, and sensor bias estimation using single observations of direction of gravitational field. *Automatica*, 125:109475, March 2021.

[13] J. Reis, P. Batista, P. Oliveira, and C. Silvestre. Attitude estimation using high-grade gyroscopes. *Control Engineering Practice*, 92:104134, November 2019.